Mathematically modeling of target speed effect on nonlinearity in DTLMI-based nano-metrology system

Saeed Olyaee[*, 1] and Masood Sherafat[1]

[1] Nano-photonics and Optoelectronics Research Laboratory (NORLab),
Shahid Rajaee Teacher Training University, Lavizan, 16788-15811,
Tehran, Iran, [*]Tel/Fax: +98-21-22970030.

Abstract: Jones matrix computation is one of the widely used methods in nonlinearity calculation in laser interferometers. In this paper, the nonlinearity error in developed three-longitudinal mode heterodyne interferometer (DTLMI) has been mathematically modeled at various speeds, by using Jones matrix calculations. This review has been done despite the fact that simultaneously the main factors including non-ideal polarization of the laser beam and the non-ideal PBS produce nonlinearity. According to the results, it was found that although nonlinearity error is a pure sinusoid in low velocities, it isn't a single-sinus and increases in amplitude in high velocities. It was also observed that the effect of non-ideal PBS on nonlinearity error is less than that of non-ideal laser beam and frequency of nonlinearity error caused by it is twice more.

1. INTRODUCTION

Today, human beings have to enter the world of nanotechnology in order to study in various fields including bio-systems and engineering science and its requirement is familiarity to measurement methods in nano-scale [1]. Using the laser interferometers is one of significant and precise methods in measurement of nanometer scale displacement, like the equipment used in fabricating the electronic chips [1, 2].

Among the laser interferometers, Michelson interferometer has been widely used in this field and according to its arrangement and number of laser modes used in it, they are classified into two categories of homodyne and heterodyne. Heterodyne interferometers have some advantages than homodyne one making

---

 * Corresponding author. Email: **s_olyaee@sru.ac.ir**

its utilization more frequent. However, its main disadvantage is nonlinearity error which influences the measurement precision [3-7].

So far, many studies have focused on nonlinearity error in a variety of heterodyne interferometers and some methods have been presented for its compensation [8-13]. Nonlinearity error in two-mode heterodyne interferometer was modelled by Cosijns *et al* in 2002 and after that, this error was studied by Olyaee *et al* by using Jones matrix calculation method, frequency-path method, and neural networks [14-18]. According to this reviews, in developed three-longitudinal mode heterodyne interferometer (DTLMI), The target displacement is obtained from measuring the phase difference created in relation to a reference state. The measured phase difference is resulting from the actual phase difference and the nonlinearity error. The nonlinearity error is mainly due to the non-ideal optical components such as laser and polarizing beam splitter (PBS) and is added as a sinusoidal sentence to the actual phase difference in accordance with the following equation [17, 19]:

$$\Delta\Phi = 4\Delta\varphi - 4k\sin\Delta\varphi \tag{1}$$

where, $\Delta\Phi$ is the measured phase difference, $\Delta\varphi$ is the actual phase difference, and k is a constant value. The nonlinearity compensation is very important to increase the resolution of nano-displacement measurement systems and we provide a way to compensation this error in [19].

It is worth pointing out that in all of these reviews, the effect of the target speed on the nonlinearity error is neglected, and in fact this error has been evaluated in low velocities of target. But it should be noted that in nanometrology, target speed is an important factor that has been neglected in previous studies. For example, in electronic chips fabricating equipment, how much can speed up, in fact productivity and output will increase. Therefore, in this research, the effect of the target speed on nonlinearity errors has been considered specially, because for offer nonlinearity error compensation method, should be specified the nature of this error and the compensation methods should be able to compensate this error at different target speeds. As shown below, speed can be a factor affecting the value and form of nonlinearity error.

In section 2, the structure of DTLMI has been reviewed and in section 3 we obtain the relations of output signals in these interferometers by using Jones calculations with regarding main factors which create nonlinearity error including non-orthogonal and elliptical polarizations in a laser beam and also non-ideal PBS. In Section 4, the effect of target speed on these relations has been studied and in section 5, nonlinearity error was obtained through the simulation. The conclusions are provided in the final section.

2. INVESTIGATION OF THE OPTICAL STRUCTURE OF DTLMI

In Fig. 1, the optical alignment and main electronic parts of DTLMI are shown [20]. In this interferometer, a laser beam is supplied by a stabilized He-Ne laser.

There are three modes with orthogonal polarization in the spectrum. The central mode with frequency ω_0 has s-polarization and two lateral modes with frequencies ω_L and ω_H have p-polarization. This laser beam is first divided into two beams by a beam splitter (BS). A beam is used to generate the reference signal and another one is directed by the second beam splitter in two routes toward fixed and movable reflectors. Although, the polarization of beam which radiates into target mirror remains unchanged after its reflection, in term of phase, it contains some information about the position of the target mirror. In other words, its phase changes as the location of target mirror changes. A beam that is radiated toward the reference mirror passes the quarter-wave plate (QWP) twice in its path and the polarization of modes of this beam change 90 degrees. In term of phase, this beam has fixed phase.

Two beams reflected from reference and target mirrors are again combined in second beam splitter (BS_2) and subsequently through a PBS, the s- and p-polarizations are directed to separate paths. In fact, ω_0 mode with target path phase and ω_L and ω_H with reference path phase having s-polarization are in the same direction. In addition, the ω_0 mode with reference path phase and ω_L and ω_H with target path phase having p-polarization are guided on another path.
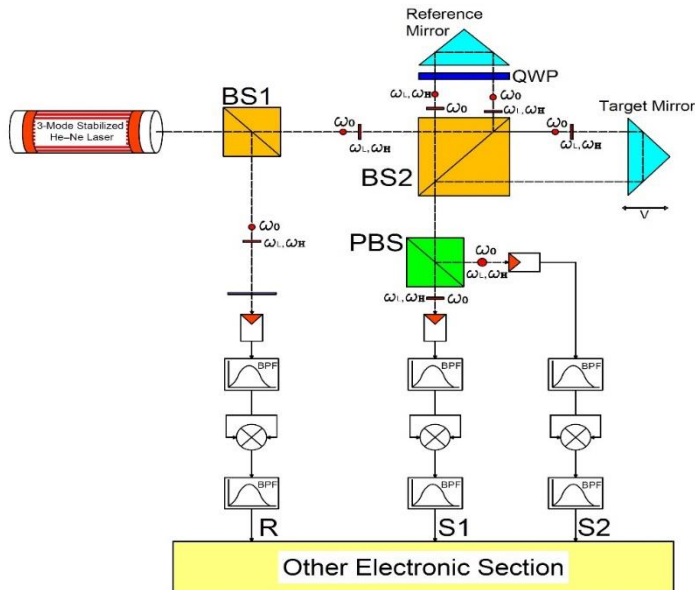

Fig. 1. Developed three-longitudinal mode heterodyne interferometer (DTLMI).

Each of these beams is converted to electrical signals by avalanche photodetectors (APDs). Then these signals are mixed with each other after

passing through the band-path filter, resulting in lowest frequency signals. Subsequently, they reach the electronic section of phase difference measurer [20].

3. THE CALCULATION OF THE ELECTRICAL SIGNALS RELATIONS AMONG VARIOUS PARTS IN DTLMI

In this section, the relations of electrical signals of various parts of DTLMI have been computed by using Jones matrix method. In these calculations, laser beam and PBS have been modeled as non-ideal while their effect on nonlinearity has been simultaneously studied.

In non-ideal conditions, the electrical fields of three-longitudinal mode laser beam are shown as:

$$\vec{E_H} = \begin{bmatrix} 1 \\ \alpha \end{bmatrix} e^{i\omega_H t}, \quad \vec{E_0} = \begin{bmatrix} \beta \\ 1 \end{bmatrix} e^{i\omega_0 t}, \quad \vec{E_L} = \begin{bmatrix} 1 \\ \alpha \end{bmatrix} e^{i\omega_L t} \tag{2}$$

where, ω_0 is the frequency of central mode, and ω_L and ω_H are the lower and higher frequencies of side modes, respectively. Also, $\alpha = |\alpha|e^{i\varphi_\alpha}$ and $\beta = |\beta|e^{i\varphi_\beta}$ implies the deviation from the ideal state of the laser beam which determines the amount of non-orthogonality and ellipticity of the polarisation states of the source. In ideal condition, these values equal zero. According to Fig. 1, Jones vector of electrical field of beams reaching PBS is calculated as:

$$\vec{E_{PBS}} = \vec{E_t} + \vec{E_r} = (Q.CCPr.Q + CCPt)$$
$$\vec{E_{in}} = \begin{bmatrix} -e^{i\Delta\varphi} & -1 \\ -1 & -e^{i\Delta\varphi} \end{bmatrix} \vec{E_{in}} \tag{3}$$

In Eq. (3), $\vec{E_{in}} = \vec{E_L} + \vec{E_0} + \vec{E_H}$ is the total electrical field vector, Q, CCP$_r$ (reference corner cube prism) and CCP$_t$ (target corner cube prism) are Jones matrix of QWP, the reference mirror, and the target mirror, respectively, which are calculated as:

$$CCP_r = \begin{bmatrix} -e^{i\Delta\varphi} & 0 \\ 0 & -e^{i\Delta\varphi} \end{bmatrix}$$
$$CCP_r = \begin{bmatrix} -1 & 0 \\ 0 & -1 \end{bmatrix} \tag{4}$$
$$Q = \frac{1}{2}\begin{bmatrix} 1-i & 1+i \\ 1+i & 1-i \end{bmatrix}$$

After passing through the PBS, each polarization of beam in direction x and y directs towards one of APDs. Therefore, vector of the electrical field that each APD receives is presented as:

$$\vec{E_{PD2}} = R.\vec{E_{PBS}}$$
$$\vec{E_{PD1}} = T.\vec{E_{PBS}} \tag{5}$$

where, T and R define transmission and reflection matrixes of PBS and in real conditions equal to $T = \begin{bmatrix} T_p & 0 \\ 0 & T_s \end{bmatrix}$ and $R = \begin{bmatrix} R_p & 0 \\ 0 & R_s \end{bmatrix}$.

The photocurrent created in any of APDs is proportional to the intensity of light falling on its surface and is obtained as:

$$I_{PD} = \overrightarrow{E_{PD}^*} \times \overrightarrow{E_{PD}} \tag{6}$$

By expanding Eq. (6) it is found that the central frequency of the band-pass filters located after APDs has been adjusted on beat frequency. The relation about the output signals of these filters is given by:

$$
\begin{aligned}
I_{BPF1} = \frac{1}{2} T_p^2 \big[& |\beta| \cos(\omega_{bL} t + \varphi_\beta) + |\alpha| \cos(\omega_{bL} t - \varphi_\alpha) \\
& + |\beta| \cos(\omega_{bH} t - \varphi_\beta) + |\alpha| \cos(\omega_{bH} t + \varphi_\alpha) \\
& + \cos(\omega_{bL} - \Delta\varphi) + |\alpha||\beta| \cos(\omega_{bL} t + \Delta\varphi + \varphi_\beta - \varphi_\alpha) \\
& + \cos(\omega_{bH} + \Delta\varphi) + |\alpha||\beta| \cos(\omega_{bH} t - \Delta\varphi + \varphi_\alpha - \varphi_\beta) \big] \\
+ \frac{1}{2} T_s^2 \big[& |\beta| \cos(\omega_{bL} t + \varphi_\beta) + |\alpha| \cos(\omega_{bL} t - \varphi_\alpha) \\
& + |\beta| \cos(\omega_{bH} t - \varphi_\beta) + |\alpha| \cos(\omega_{bH} t + \varphi_\alpha) \\
& + \cos(\omega_{bL} + \Delta\varphi) + |\alpha||\beta| \cos(\omega_{bL} t - \Delta\varphi + \varphi_\beta - \varphi_\alpha) \\
& + \cos(\omega_{bH} - \Delta\varphi) + |\alpha||\beta| \cos(\omega_{bH} t + \Delta\varphi + \varphi_\alpha - \varphi_\beta) \big]
\end{aligned}
\tag{7}
$$

The relation of I_{BPF2} is also similar to the Eq. (7) with the exception that T_p and T_s are replaced by R_p and R_s, respectively. In Eq. (7), $\omega_{bH} = \omega_H - \omega_0$ and $\omega_{bL} = \omega_0 - \omega_L$ which are called beat frequencies and whose values are different in various lasers. they vary usually from 250MHz to 1GHz.

After passing these signal through mixers and band-pass filters, final relations are presented as:

$$
\begin{aligned}
S_1 = \frac{1}{8} \big[& A \cos(\omega_b t - 2\varphi_\beta) + B \cos(\omega_b t + \varphi_\alpha - \varphi_\beta) + C \cos(\Delta\varphi + \varphi_\beta) \\
& + D \cos(\Delta\varphi - \varphi_\beta) + E \cos(\Delta\varphi + \varphi_\alpha) + F \cos(\Delta\varphi - \varphi_\alpha) \\
& + G \cos(\omega_b t - \Delta\varphi - \varphi_\beta) + H \cos(\omega_b t + \Delta\varphi - \varphi_\beta) \\
& + I \cos(\omega_b t - \Delta\varphi + \varphi_\alpha - 2\varphi_\beta) \\
& + J\cos(\omega_b t + \Delta\varphi + \varphi_\alpha - 2\varphi_\beta) + K \cos(\omega_b t + 2\varphi_\alpha) \\
& + L \cos(\omega_b t - \Delta\varphi + \varphi_\alpha) + M \cos(\omega_b t + \Delta\varphi + \varphi_\alpha) \\
& + N\cos(\omega_b t - \Delta\varphi + 2\varphi_\alpha - \varphi_\beta) \\
& + O\cos(\omega_b t + \Delta\varphi + 2\varphi_\alpha - \varphi_\beta) + P\cos(2\Delta\varphi) \\
& + Q\cos(2\Delta\varphi - \varphi_\alpha + \varphi_\beta) + R\cos(\omega_b t) \\
& + S\cos(\omega_b t + 2\Delta\varphi) + T\cos(\omega_b t + 2\Delta\varphi + \varphi_\alpha - \varphi_\beta) \\
& + U\cos(2\Delta\varphi + \varphi_\alpha - \varphi_\beta) + V\cos(\omega_b t - 2\Delta\varphi) \\
& + W\cos(\omega_b t - 2\Delta\varphi + \varphi_\alpha - \varphi_\beta) \\
& + X\cos(\omega_b t + 2\varphi_\alpha - 2\varphi_\beta) \\
& + Y\cos(\omega_b t + 2\Delta\varphi + 2\varphi_\alpha - 2\varphi_\beta) \\
& + Z\cos(\omega_b t - 2\Delta\varphi + 2\varphi_\alpha - 2\varphi_\beta) \big]
\end{aligned}
\tag{8}
$$

where, the coefficients of Eq. (8) are listed in Table I.

Relation S_2 is similar to S_1 with the exception that T_p and T_s are replaced by R_p and R_s., respectively. By similar calculations, the relation of reference signal (R) is obtained as:

$$
\begin{aligned}
R = \frac{1}{2}\big[&\cos(\omega_b t) + 2|\alpha|\cos(\omega_b t + \varphi_\alpha) + 2|\beta|\cos(\omega_b t - \varphi_\beta) \\
&+ |\alpha|^2\cos(\omega_b t + 2\varphi_\alpha) + |\beta|^2\cos(\omega_b t - 2\varphi_\beta) \\
&+ 4|\alpha||\beta|\cos(\omega_b t + \varphi_\alpha - \varphi_\beta) \\
&+ 2|\alpha||\beta|^2\cos(\omega_b t + \varphi_\alpha - 2\varphi_\beta) \\
&+ 2|\alpha|^2|\beta|\cos(\omega_b t + 2\varphi_\alpha - \varphi_\beta) \\
&+ |\alpha|^2|\beta|^2\cos(\omega_b t + 2\varphi_\alpha - 2\varphi_\beta)\big]
\end{aligned}
\tag{9}
$$

TABLE I
COEFFICIENTS OF EQ. (8)

COEFFICIENT	VALUE
A	$|\beta|^2\big(T_p^2 + T_s^2\big)^2$
B	$4|\alpha||\beta|\big(T_p^2 + T_s^2\big)^2 - 4|\alpha||\beta|T_p^2 T_s^2$
C	$2T_p^2|\beta|(|\alpha|^2 + 1)\big(T_p^2 + T_s^2\big)$
D	$2T_s^2|\beta|(|\alpha|^2 + 1)\big(T_p^2 + T_s^2\big)$
E	$2T_s^2|\alpha|(|\beta|^2 + 1)\big(T_p^2 + T_s^2\big)$
F	$2T_p^2|\alpha|(|\beta|^2 + 1)\big(T_p^2 + T_s^2\big)$
G	$2T_s^2|\beta|\big(T_p^2 + T_s^2\big)$
H	$2T_p^2|\beta|\big(T_p^2 + T_s^2\big)$
I	$2T_p^2|\alpha||\beta|^2\big(T_p^2 + T_s^2\big)$
J	$2T_s^2|\alpha||\beta|^2\big(T_p^2 + T_s^2\big)$
K	$|\alpha|^2\big(T_p^2 + T_s^2\big)^2$
L	$2T_s^2|\alpha|\big(T_p^2 + T_s^2\big)$
M	$2T_p^2|\alpha|\big(T_p^2 + T_s^2\big)$
N	$2T_p^2|\alpha|^2|\beta|\big(T_p^2 + T_s^2\big)$
O	$2T_s^2|\alpha|^2|\beta|\big(T_p^2 + T_s^2\big)$
P	$2T_p^2 T_s^2(1 + |\alpha|^2|\beta|^2)$
Q	$2T_p^4|\alpha||\beta|$
R	$2T_p^2 T_s^2$
S	T_p^4
T	$2T_p^2 T_s^2|\alpha||\beta|$
U	$2T_s^4|\alpha||\beta|$
V	T_s^4
W	$2T_p^2 T_s^2|\alpha||\beta|$
X	$2T_p^2 T_s^2|\alpha|^2|\beta|^2$
Y	$T_s^4|\alpha|^2|\beta|^2$
Z	$T_p^4|\alpha|^2|\beta|^2$

In Eqs. (8) and (9), $\omega_b = \omega_{bH} - \omega_{bL}$ which is called secondary beat frequency is usually about 300 kHz [15-16, 20].

4. STUDY THE EFFECT OF TARGET VELOCITY ON RELATIONS S_1 AND S_2

Some terms in the S_1 and S_2 relationships depends on the target velocity. Since $\Delta\varphi$ is proportional to target displacement, it is in fact a time-depended

term. Depending on the target velocity, terms in equations S_1 and S_2 including $\Delta\varphi$ are omitted or passed by band-pass filter. Assuming that pass band of band-pass filters located after mixers is designed in 200 kHz – 5 MHz. Table II shows terms that are eliminated at any range of velocity. This table is set for the velocities in the positive direction (Doppler frequency increase) and the eliminated coefficients are the coefficients of the relation S_1. The same conditions are considered for negative velocities. Here, similar sentences in relation S_2 are omitted.

TABLE II
ELIMINATED COEFFICIENTS OF RELATION S₁ AT VARIOUS RANGES OF VELOCITY

Velocity range	Equivalent Doppler frequency	Deleted coefficients of relation s_1
Less than $16\frac{mm}{s}$	Less than 50KHz	Sentences with coefficients C , D , E , F , P , Q , U
$16\frac{mm}{s}$ - $32\frac{mm}{s}$	50KHz- 100KHz	Sentences with coefficients C , D , E , F , P , Q , U , V , W , Z
$32\frac{mm}{s}$ - $64\frac{mm}{s}$	100KHz - 200KHz	Sentences with coefficients C , D , E , F , G , I , L , N , V , W , Z
$64\frac{mm}{s}$ - $80\frac{mm}{s}$	200KHz - 250KHz	Sentences with coefficients G , I , L , N , V , W , Z
$80\frac{mm}{s}$ - $160\frac{mm}{s}$	250KHz - 500KHz	Sentences with coefficients G, I , L , N
$160\frac{mm}{s}$ - $1.5\frac{m}{s}$	500KHz - 4.85MHz	None of them

5. RESULTS

By converting S_1, S_2, and R signals to the square signals and measuring the phase difference among them, we can calculate the displacement of the target. For low velocities, the phase difference between S_1, S_2 and for high velocities, the phase difference between R and either S_1 or S_2 signal is measured. By comparing the measured displacement to real displacement, nonlinearity error is obtained.

Nonlinearity error for various intervals of velocity was computed as shown in Table 2 and it was observed that the nonlinearity error curve for velocities less than 64mm/s is different with velocities more than 64mm/s. For the velocities less than 64mm/s, nonlinearity error is as a pure sinus but for velocities higher than this, the shape of nonlinearity error changes and its amplitude increases. Of course, velocity 64mm/s depends on band-pass filter bandwidth and changes as passband of filter changes.

Curves in Fig. 2 show the nonlinearity error for these two velocity intervals. As depicted in Fig. 2, conditions exerted for non-ideal states are derived from datasheet of manufacturers of laser and PBS. Then the worst condition has been

selected among them. Table III shows the maximum nonlinearity error in different speed intervals at worst condition.
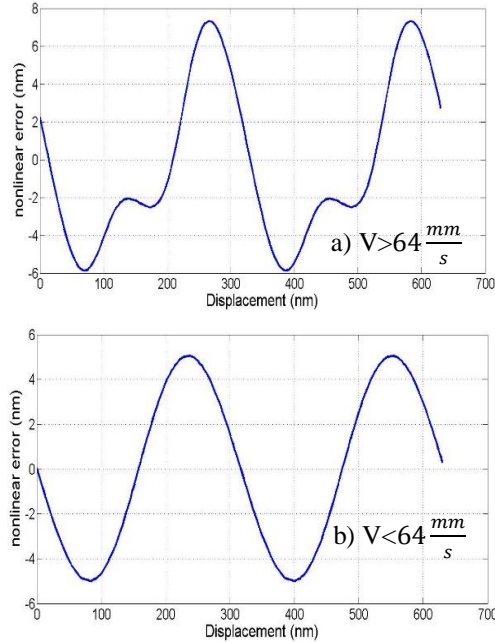

Fig. 2. Nonlinearity error for two velocity intervals with conditions T_p=0.95, T_s=0.01, $|\alpha| = |\beta|$ =0.05, $\varphi_\alpha = \varphi_\beta = 0.1$

TABLE III
MAXIMUM NONLINEARITY ERROR IN DIFFERENT SPEED INTERVALS

Velocity range $(\frac{mm}{s})$	Maximum nonlinearity error (nm)
Less than 16 $\frac{mm}{s}$	5.048
16 - 32	5.048
32 - 64	4.937
64 - 80	7.327
80 - 160	7.328
160 - 1.5	7.329

To examine the impact of each factor causing the nonlinearity error, two cases have been considered. First, while laser beam is ideal, the effect of non-ideal PBS on nonlinearity error has been studied. Second, while PBS is considered as ideal, the effect of non-ideal laser beam on nonlinearity error has been investigated. In

two states, simulations have been done for two velocity intervals, i.e. velocities less and more than 64mm/s, respectively, as depicted in Figs. 3 and 4.

It can be found from curves of Figs. 2 and 3 that if the source of nonlinearity error is only non-ideal PBS, the frequency of nonlinearity error is twice more so non-ideal PBS plays less role in nonlinearity. According to curves in Figs. 3 and 4, it is observed that in high velocities, the amplitude of nonlinearity error will increase and also a shift is seen in its curve.
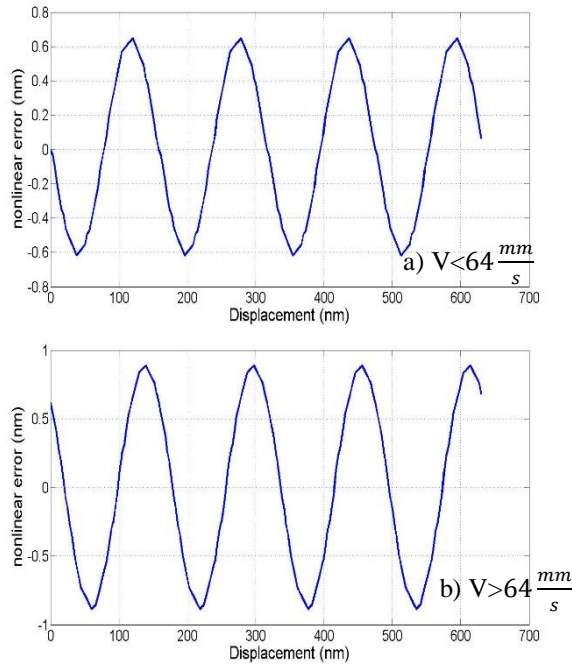
Fig. 3. Nonlinearity error caused by non-ideal PBS at high and low velocities at conditions T_p=0.9, T_s=0.1, R_p=0.1, R_s=0.9.

From among the two T_p and T_s parameters which are effective in positive velocities, parameter T_s was more effective, as shown in Fig. 5. The slope of the curve in the direction of the T_s axis is greater than the curve slope in T_p direction.

Also, Fig. 6 shows that the effect of T_s is more at higher speeds. The curve of Fig. 6 represents the effect of T_s parameter on nonlinearity error at different velocities.
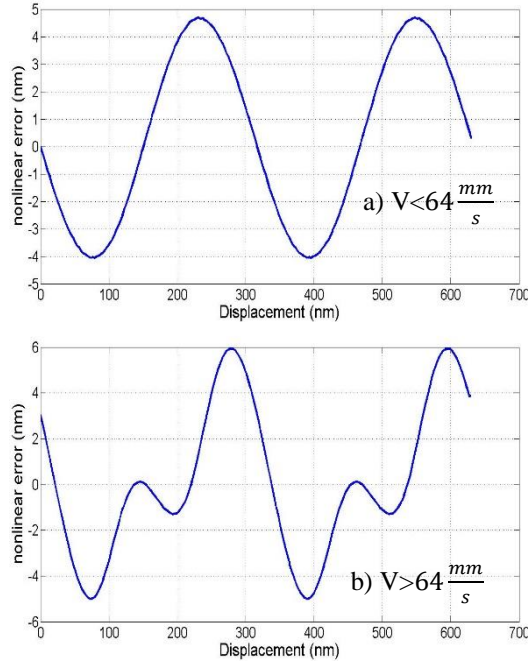
Fig. 4. Nonlinearity error caused by non-ideal laser beam at high and low velocities at conditions $\varphi_\alpha = .45$, $\varphi_\beta = .6$, $|\alpha| = |\beta| = .05$

6. CONCLUSION

In this study, the effect of speed on nonlinearity error in heterodyne interferometers has been studied for the first time. The nonlinearity resulting from non-ideal PBS and laser beam have been mathematically modeled and simulated by Jones matrix method. According to the provided results, it has been found that target velocity affects the nonlinearity because of band-pass filter. Duo to the Doppler frequency, the frequency of some terms mentioned earlier in output relations of mixers depends on velocity. These terms can be deleted by band-pass filter or passed over it. Such performed simulations, in the velocities higher than a determined limit depending on pass band of band-pass filter, nonlinearity error will be increased result in changing its pure sinus form. In addition, the lower cutoff frequency of the filter has the most effect in this regard and since the secondary beat frequency is little, lower cutoff frequency of filter cannot be significantly increased. In the simulations, effect of two main factors of nonlinearity error including non-ideal laser and PBS was studied. According to these investigations, effect of non-ideal laser on nonlinearity error is more than non-ideal PBS. Moreover, it was found that the nonlinearity error frequency derived from non-ideal PBS is twice more than that of non-ideal laser.
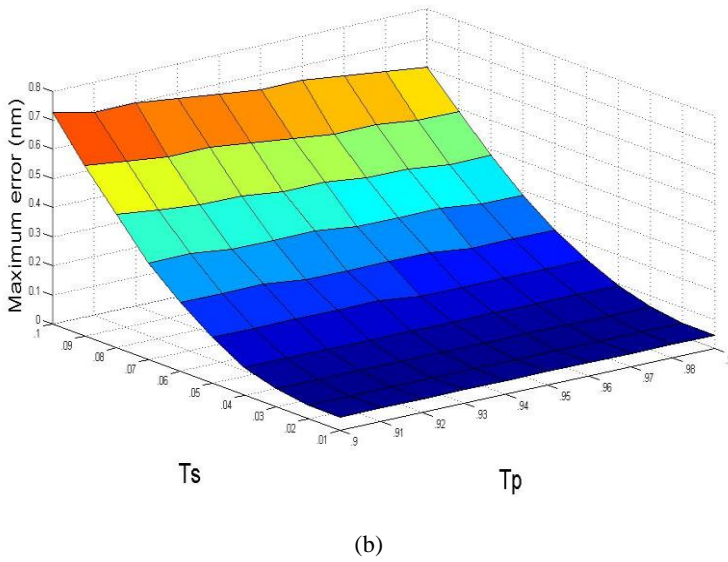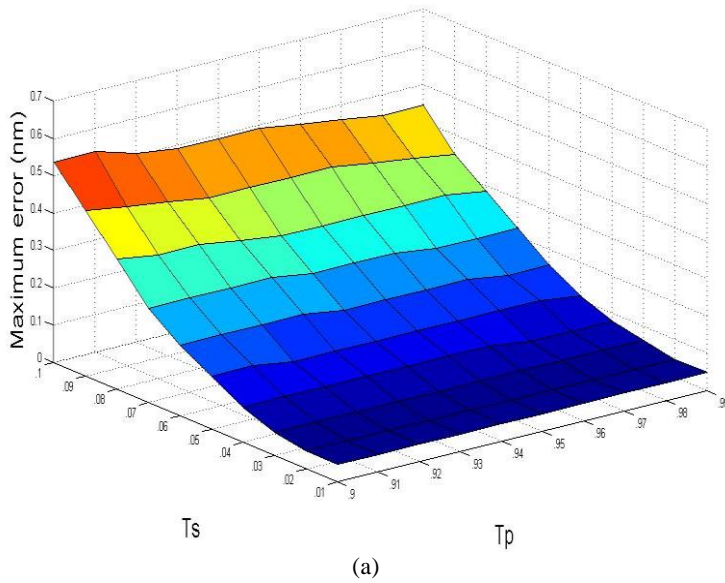
(a)

(b)

Fig. 5. Effect of T_p and T_s on the nonlinearity error at (a) low and (b) high velocities.
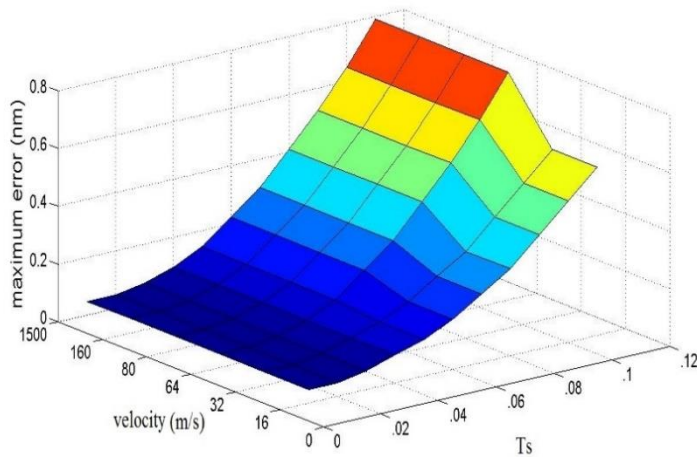
Fig. 6. Effect of T$_s$ on the nonlinearity error at different velocities.

REFERENCES

[1] M. L. Schattenburg and I. H. Smith. *The critical role of metrology in nanotechnology*. Proc. SPIE, 4608(1) (2002) 116-124.
Available:https://www.spiedigitallibrary.org/conference-proceedings-of-pie/4608/1

[2] F. C. Demarest. *High-resolution, high-speed, low data age uncertainty, heterodyne displacement measuring interferometer electronics*. Meas. Sci. Technol. 9(7) (1998) 1024-1030.
Available: http://iopscience.iop.org/article/10.1088/0957-0233/9/7/003

[3] W. Estler, Tyler. *High-accuracy displacement interferometry refin air*. Appl. Opt. 24(6) (1985) 808-815.
Available: https://www.osapublishing.org/ao/abstract.cfm?uri=ao-24-6-808

[4] N. Bobroff, Norman. *Recent advances in displacement measuring interferometry*. Meas. Sci. Technol. 4(9) (1993) 907-926.
Available: http://iopscience.iop.org/article/10.1088/0957-0233/4/9/001

[5] W. Hou, and Günter Wilkening. *Investigation and compensation of the nonlinearity of heterodyne interferometers*. Precision Eng. 14(2) (1992) 91-98.
Available: https://www.sciencedirect.com/science/article/pii/014163599290054Z

[6] K. Chen, Jing-Heng Chen, Shen-Hua Lu, Wei-Yao Chang, and Chi-Chang Wu. *Absolute distance measurement by using modified dual-wavelength heterodyne Michelson interferometer*. Opt. Commun. 282(9) (2009) 1837-1840.
Available: https://www.sciencedirect.com/science/article/pii/S003040180900042X

[7] A. Rezaei, B. Azizollah-Ganji, and M. Gholipour. *Effects of the channel length on the nanoscale field effect diode performance*. J. Optoelectronical Nanostructures. 3(2) (2018) 29-39.
Available: http://jopn.miau.ac.ir/article_2862.html

[8] A. Ju, Chaoyang Zhong, and Wenmei Hou. *The effect of laser source and PBS on the nonlinearity in heterodyne interferometer*. Optik-International Journal for Light and Electron Optics. 126(1) (2015) 112-115.
Available: https://www.sciencedirect.com/science/article/pii/S0030402614011978

[9] H. Hu, and Juju Hu. *Relations between nonlinearity and PBS in heterodyne Michelson interferometer with different optical structures*. Optik-International Journal for Light and Electron Optics, 126(24) (2015) 5061-5066.
Available: https://www.sciencedirect.com/science/article/pii/S0030402615012036

[10] W. Hou. *Optical parts and the nonlinearity in heterodyne interferometers*. Precision Eng. 30(3) (2006) 337-346.
Available: https://www.sciencedirect.com/science/article/pii/S0141635905001637

[11] J. Guo, Yan Zhang, and Shuai Shen. *Compensation of nonlinearity in a new optical heterodyne interferometer with doubled measurement resolution*. Opt. Commun. 184(1) (2000) 49-55.
Available: https://www.sciencedirect.com/science/article/pii/S0030401800009342

[12] W. Hou, Yunbo Zhang, and Haijiang Hu. *A simple technique for eliminating the nonlinearity of a heterodyne interferometer*. Meas. Sci. Technol. 20(10) (2009). 105303.
Available: http://iopscience.iop.org/article/10.1088/0957-0233/20/10/105303/meta

[13] S. Olyaee, R. Ebrahimpour, and S. Hamedi. *Modeling and compensation of periodic nonlinearity in two-mode interferometer using neural networks*. IETE J. Research. 56(2) (2010). 102-110.
Available: https://www.tandfonline.com/doi/abs/10.4103/0377-2063.63085

[14] S. J. A. G. Cosijns, Han Haitjema, and P. H. J. Schellekens. *Modeling and verifying non-linearities in heterodyne displacement interferometry*. Precision Eng. 26(4) (2002) 448-455.
Available: https://www.sciencedirect.com/science/article/pii/S0141635902001502

[15] S. Olyaee, S., and S. Mohammad Nejad. *Nonlinearity and frequency-path modelling of three-longitudinal-mode nanometric displacement measurement system*. IET Optoelectron. 1(5) (2007). 211-220.
Available: https://ieeexplore.ieee.org/document/4312812/

[16] S. Olyaee, T. H. Yoon, and S. Hamedi. *Jones matrix analysis of frequency mixing error in three-longitudinal-mode laser heterodyne interferometer*. IET Optoelectron. 3(5) (2009) 215-224.
Available: https://ieeexplore.ieee.org/document/5235434/

[17] S. Olyaee, and S. Hamedi. *A low-nonlinearity laser heterodyne interferometer with quadrupled resolution in the displacement measurement*. Arab. J. Sci. Eng. 36(2) (2011) 279-286.
Available: https://link.springer.com/article/10.1007/s13369-010-0017-5

[18] S. Olyaee, S. Hamedi, and Z. Dashtban. *Efficient performance of neural networks for nonlinearity error modeling of three-longitudinal-mode interferometer in nano-metrology system*. Precision Eng. 36(3) (2012) 379-387.
Available: https://www.sciencedirect.com/science/article/pii/S0141635912000037

[19] M. Sherafat and S. Olyaee. *A nonlinearity error compensation method in nano-metrology system based on developed three-longitudinal mode heterodyne interferometer*. Int. J. Mechatronics Appl. Mechanics. 3 (2018) 60-65.
Available: https://ijomam.com/issue3

[20] S. Yokoyama, T. Yokoyama, and T. Araki. *High-speed subnanometre interferometry using an improved three-mode heterodyne interferometer*. Meas. Sci. Technol. 16(9) (2005) 1841-1847.
Available: http://iopscience.iop.org/article/10.1088/0957-0233/16/9/017